

# Study of Mach 0.8 Transonic Truss-Braced Wing Aircraft Wing-Strut Interference Effects

Juntao Xiong<sup>1</sup>

KBR Wyle, *Inc.*, Moffett Field, CA 94035

Nhan Nguyen<sup>2</sup>

NASA Ames Research Center, Moffett Field, CA 94035

Jason Fugate<sup>3</sup>

KBR Wyle, *Inc.*, Moffett Field, CA 94035

**This paper presents a computational study of transonic wing-strut interference effects of the Mach 0.8 Transonic Truss-Braced Wing (TTBW) aircraft using the high-fidelity CFD solver FUN3D. The study is conducted for the wing-strut and the wing-alone configurations at design Mach number 0.8 and Reynolds number  $14.0 \times 10^6$ . The interference effects are calculated by comparing the wing aerodynamics along the spanwise direction between the wing-strut and the wing-alone configurations. The presence of the strut underneath the wing induces a suction peak on the lower surface of the wing, which causes changes in aerodynamic forces and moments. The interference effects of the Mach 0.8 TTBW aircraft are compared with the Mach 0.745 TTBW aircraft. A transonic wing-strut interference aerodynamic correction model is developed for use in a lower-fidelity tool, VSPAERO, for rapid aerodynamic analysis of the Mach 0.8 TTBW aircraft.**

## I. Introduction

The Subsonic Ultra Green Aircraft Research (SUGAR) Transonic Truss-Braced Wing (TTBW) aircraft concept is a Boeing-developed N+3 aircraft configuration funded by NASA Aeronautics Research Mission Directorate (ARMD) Advanced Air Transport Technologies (AATT) project.<sup>1-3</sup> The TTBW aircraft concept is designed to be aerodynamically efficient by employing a wing aspect ratio of about 19.55, which is significantly greater than those of cantilever wing transport configurations. Figure 1 is an illustration of the TTBW aircraft. Without structural bracing, the increase in the wing root bending moment would require a significant structural reinforcement which would lead to an increase in the structural weight that would offset the aerodynamic benefit of the high aspect ratio wing. Thus, the design of a truss-braced structure is a Multidisciplinary Design Optimization (MDO) process that strives to achieve a delicate balance between aerodynamic efficiency and structural efficiency. A typical MDO process uses a variety of different tools of varying fidelity for many different purposes such as aerodynamic prediction, aero-structural analysis, flutter analysis. Computational Fluid Dynamics (CFD) is the main tool for aerodynamic prediction. On the other hand, for flight dynamic analysis of stability and control, a lower-order tool may be sufficient during the early stage of the design.

---

<sup>1</sup> Aerospace Engineer, Intelligent System Division, [juntao.xiong@nasa.gov](mailto:juntao.xiong@nasa.gov), AIAA Member

<sup>2</sup> Senior Research Scientist, Intelligent System Division, [nhan.t.nguyen@nasa.gov](mailto:nhan.t.nguyen@nasa.gov), Associate Fellow AIAA

<sup>3</sup> Aerospace Engineer, Intelligent System Division, [jason.fugate@nasa.gov](mailto:jason.fugate@nasa.gov)



**Figure 1. Boeing SUGAR Truss-Braced Wing (TBW) Aircraft Concept**

A previous study was conducted to investigate the aerodynamic and structural performances of the Mach 0.745 TTBW aircraft by using a fast low-fidelity potential flow solver VSPAERO coupled with an in-house nonlinear finite-element code BEAM3D.<sup>4</sup> The VSPAERO code includes both a low-fidelity vortex-lattice model and a mid-fidelity panel model for steady-state aerodynamics. Transonic and viscous flow corrections for the steady-state aerodynamics are implemented on the vortex-lattice model using a 2D transonic small disturbance (TSD) code called TSFOIL coupled to an in-house integral boundary layer (IBL) code. In the region near the strut attachment to the wing, the flow involves a considerable degree of 3D transonic and viscous interactions between the wing and the strut. A high-fidelity CFD model of the Mach 0.745 TTBW aircraft was developed using FUN3D to investigate the wing-strut interference aerodynamics for the purpose of developing a wing-strut interference aerodynamic correction method to be applied to the VSPAERO model. Upon applying all the necessary corrections, the VSPAERO model shows an excellent agreement with wind tunnel test data for the Mach 0.745 TTBW aircraft.<sup>5</sup>

In this paper the high-fidelity CFD solver FUN3D is used to investigate the impact of the 3D transonic and viscous interference for the aircraft developed by Boeing under a Phase IV NRA (NASA Research Announcement) contract funded by NASA AATT project. First, the CFD solver FUN3D simulation results of the Mach 0.8 TTBW aircraft are validated with NASA Ames 11-Ft transonic wind tunnel experimental measurements. Then, the FUN3D solver is used to simulate the wing-strut and wing-alone configurations to investigate the transonic interference effects of the Mach 0.8 TTBW aircraft. The interference effects of the Mach 0.8 TTBW aircraft are compared with the Mach 0.745 TTBW aircraft. Based on the simulation results, an interference correction model is developed for the VSPAERO solver to improve the predictive capability of the VSPAERO for the Mach 0.8 TTBW aircraft.

## **II. Computational Approach**

### **A. Numerical Code**

The computational fluid dynamics code used in this study is FUN3D<sup>6-7</sup>, which solves the unsteady 3D Navier-Stokes equations on mixed-element grids using a vertices-centered finite-volume method. Information exchange for flow computation on different partitions using multiple CPUs is implemented through the Message Passing Interface (MPI) protocol. It employs an implicit upwind algorithm in which the inviscid fluxes are obtained with a flux-difference-splitting scheme. At interfaces delimiting neighboring control volumes, the inviscid fluxes are computed using an approximate Riemann solver based on the values on either side of the interface. The Roe's flux difference splitting<sup>8</sup> is used in the current study. For second-order accuracy, interface values are obtained by extrapolation of the control volume centroidal values, based on gradients computed at the mesh vertices, using an unweighted least-squares technique.

The Venkatakrishnan<sup>9</sup> limiter is used in the current study to limit the reconstructed values when necessary. In this study a tetrahedral with prism meshes is used. In FUN3D, for tetrahedral meshes, the full viscous fluxes are discretized using a finite-volume formulation in which the required velocity gradients on the dual faces are computed using the Green-Gauss theorem. The solution at each time-step is updated with a backwards Euler time-differencing scheme. At each time step, the system of equations is approximately solved with either a multi-color point-implicit procedure or an implicit-line relaxation scheme. Local time-step scaling is employed to accelerate convergence to steady-state. To model turbulent flows, the one-equation model of Spalart-Allmaras<sup>10</sup> (S-A) is used in this study.

## B. Computational Model and Grid

In this paper, the Mach 0.8 TTBW aircraft 1g shape geometry is studied. Wind tunnel tests have been conducted in NASA Ames 11-Ft Transonic Wind Tunnel. First, two configurations of the Mach 0.8 TTBW aircraft geometry are used for the simulation validation. Figure 2 illustrates the Mach 0.8 TTBW geometry config-137, which includes all the aircraft components except horizontal tail and jury strut. Figure 3 shows the surface mesh of the geometry. The volume mesh is comprised of tetrahedral elements and a prism layer near the wall. The mesh size is about 96 million nodes. The prism layer is used to resolve the turbulent boundary layer. The  $y^+$  of the first cell from the wall is less than 1.

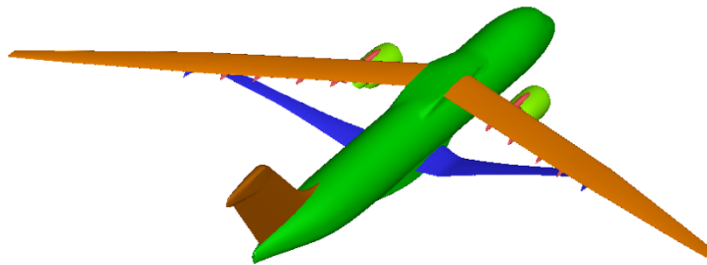


**Fig. 2 Mach 0.8 TTBW Geometry config-137**

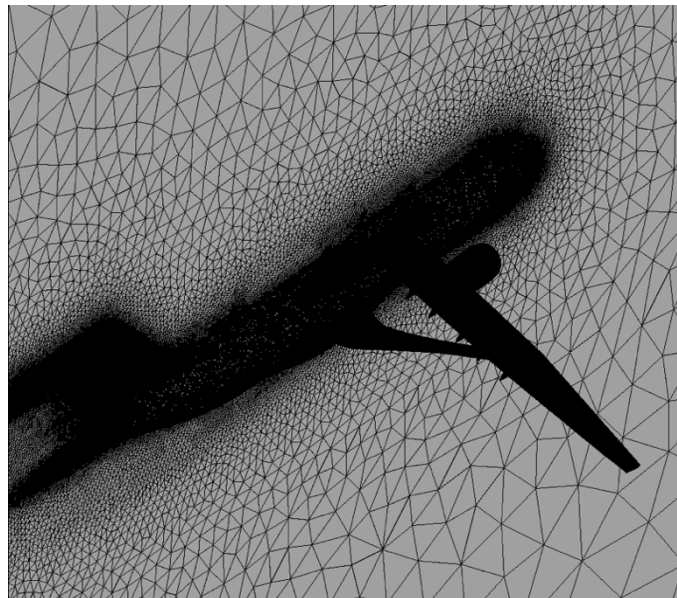


**Fig. 3 Computational Grid**

After validation, the wing-strut interference effects are studied for the Mach 0.8 TTBW aircraft. In this paper, in order to save the computation expenses the engine and the horizontal tail are not modelled since we only focus on studying the wing-strut interference effects. Figure 4 shows the wing-alone and wing-strut configurations of the Mach 0.8 TTBW geometry which are used to investigate the interference effects.

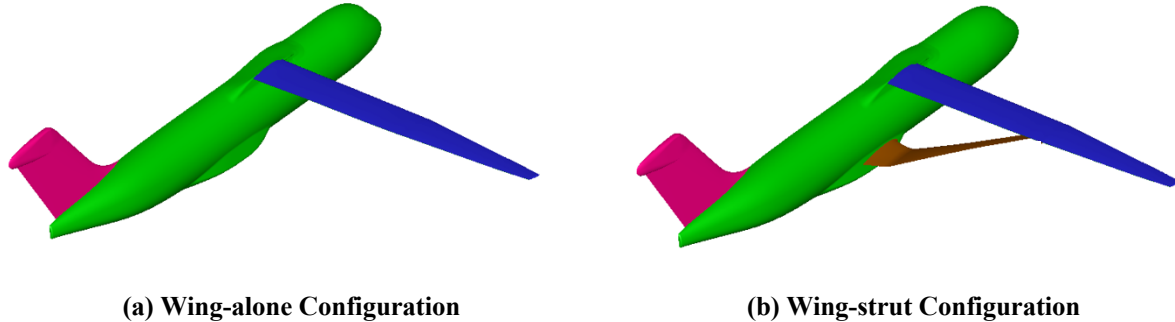


**Fig. 4 Mach 0.8 TTBW Configurations**

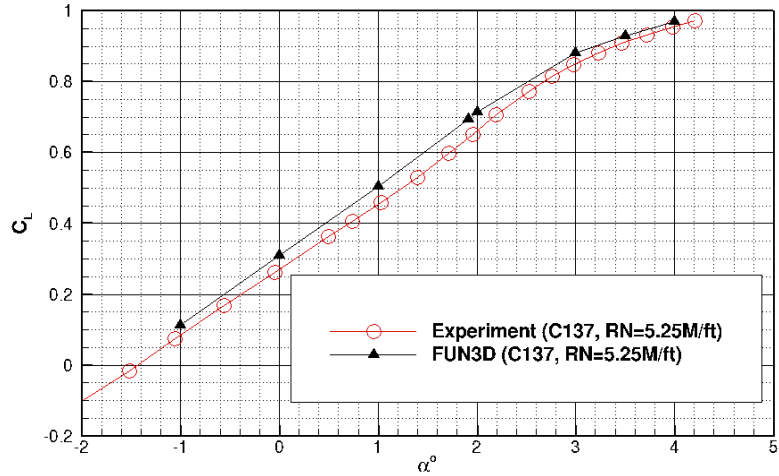
### III. Results

First the computation results are validated with experimental data for the Mach 0.8 TTBW geometry config-137 and config-121. The config-121 geometry does not include the engine/pylon, horizontal tail, and jury strut. Wind tunnel test data of the Mach 0.8 TTBW model in NASA Ames 11-Ft Transonic Wind Tunnel are available for validation. Test data from Run 378 at Mach 0.8 and Reynolds number of 2.17 million based on the mean aerodynamic chord (MAC) with full wind tunnel model corrections are used for the config-137 validation. Test data from Run 433 at Mach 0.8 and Reynolds number of 2.17 million based on the MAC with full wind tunnel model corrections are used for the config-121 validation. After the validation, FUN3D code is used to simulate the wing-alone and wing-strut configurations which are shown in Fig. 4 and to determine the interference effects at design Mach number 0.8 and Reynolds number  $14.0 \times 10^6$ . The interference effects of the Mach 0.8 TTBW aircraft are quantitatively compared with the Mach 0.745 TTBW aircraft. Based on the simulation results, an interference correction model is developed for the VSPAERO code.

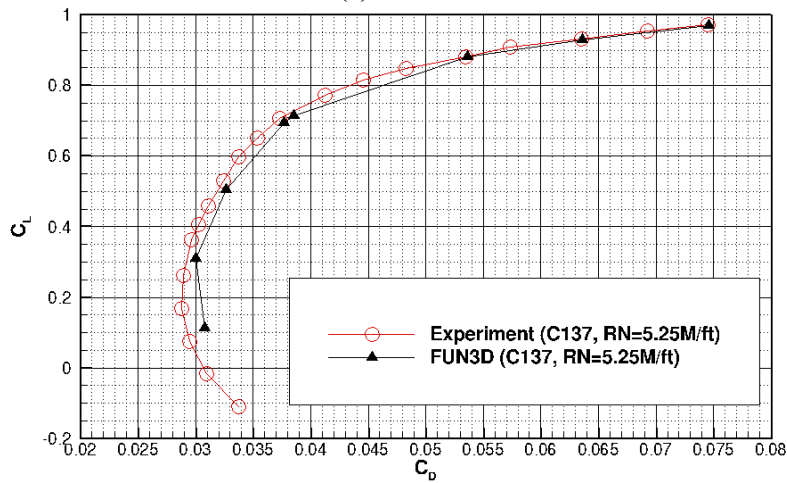
#### A. CFD Solver Validation

The presentation of the results begins with a comparison between aerodynamic forces obtained both experimentally from a recently completed wind tunnel test in the NASA Ames 11-By-11-Foot Transonic Wind Tunnel, and computationally via FUN3D for the Mach 0.8 TTBW geometry config-137 for Mach 0.8 and a Reynolds number of 2.17 million. Figure 5 shows the lift and drag coefficients computed by FUN3D as well as Run 378 wind tunnel data. Compared to the experimental data, FUN3D slightly overpredicts the lift coefficient. There is an angle of attack shift of approximately 0.23 degrees at the design lift coefficient of 0.695. The drag polar computed by FUN3D shows good agreement with the wind tunnel data. The difference in the drag coefficient at the design lift coefficient of 0.695 is about 8 counts. The discrepancy in the drag coefficient progressively becomes larger at lower lift coefficients. Figure 6 shows the surface pressure coefficient distribution at one simulated flight condition of config-137. There is a weak shock structure on the wing, which helps to improve the lift coefficient with a small drag penalty at transonic conditions. To further validate the FUN3D simulation results, another set of Run 433 wind tunnel data for config-121 is used. Figure 7 shows the lift and drag coefficients computed by FUN3D as well as Run 433 wind tunnel data of the Mach 0.8 TTBW geometry config-121 for Mach 0.8 and a Reynolds number of

2.17 million. Similar to the config-137 comparison, FUN3D also overpredicts the lift coefficient for config-121. There is an angle of attack shift of approximately 0.27 degrees at the design lift coefficient 0.695. The reasons of the offset of the lift curves need to be further investigated. The drag polar computed by FUN3D shows a very good agreement with the wind tunnel data especially at a lift coefficient at or greater than the design lift coefficient of 0.695. Figure 8 shows the surface pressure coefficient distribution at one simulated flight condition of config-121. The close agreements with wind tunnel data provide confidence in the FUN3D prediction for further investigating the transonic wing-strut interference effects.



(a) Lift Curve



(b) Drag Polar

**Fig. 5 Comparison of Lift and Drag Predictions for the TTBW Geometry Config-137 ( $M_\infty = 0.8$ ,  $Re = 2.17 \times 10^6$ )**

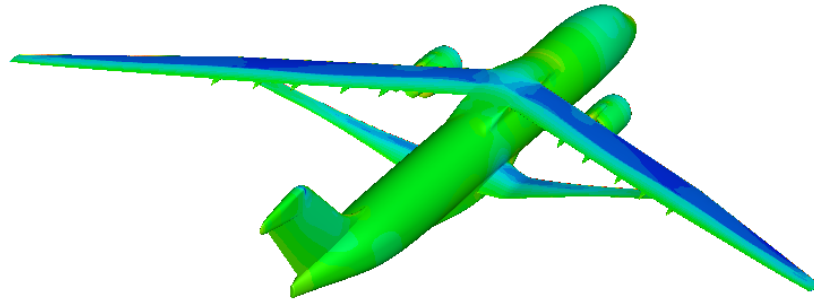
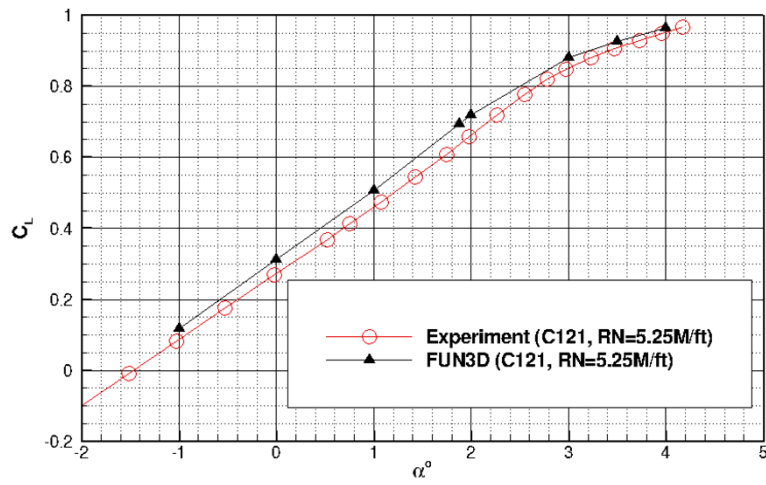
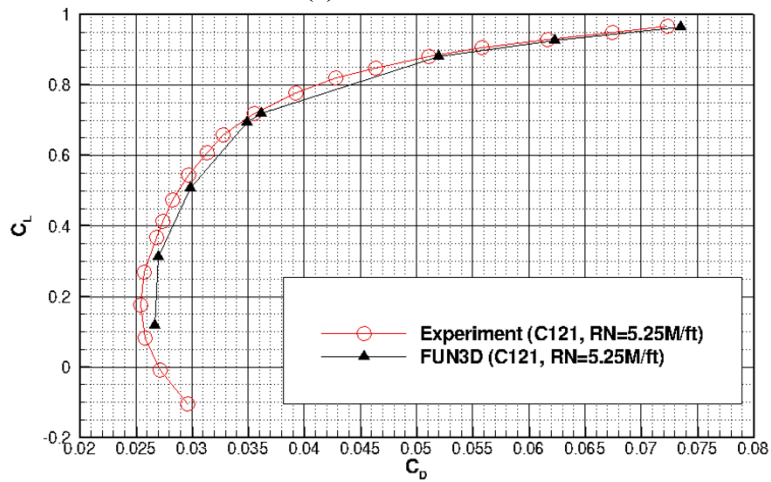


**Fig. 6 Pressure Coefficient Contour on the TTBW Geometry Config-137 Surface**  
 $(M_\infty = 0.8, C_L = 0.695, Re = 2.17 \times 10^6)$



**(a) Lift Curve**



**(b) Drag Polar**

**Fig. 7 Comparison of Lift and Drag Predictions for the TTBW Geometry Config-121**  
 $(M_\infty = 0.8, Re = 2.17 \times 10^6)$

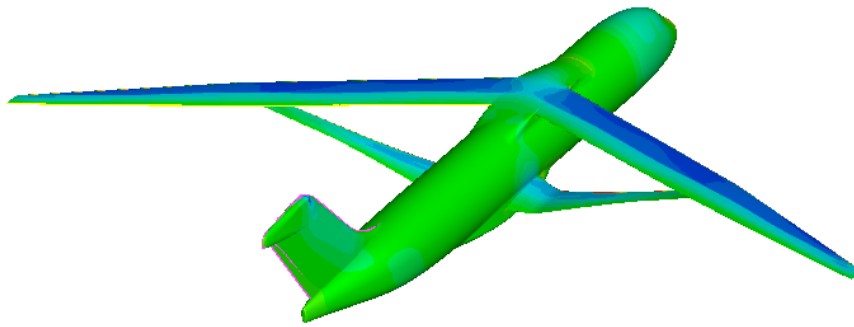


**Fig. 8 Pressure Coefficient Contour on the TTBW Geometry Config-121 Surface**  
 $(M_\infty = 0.8, C_L = 0.695, Re = 2.17 \times 10^6)$

### B. Wing-strut Interference Effects

The wing-strut interference effects are investigated by determining the difference in the wing sectional aerodynamic coefficients between the wing-alone and the wing-strut configurations which are shown in Fig. 4.

Figures 9 show the pressure coefficient distributions at five wing span locations at  $1.533^\circ$  angle of attack for Mach number 0.8 and Reynolds number 14.0 million. The pressure distributions for the wing-alone configuration are not shown in the figures. The pressure differences between the wing-alone and wing-strut configurations are small at the inboard of the wing where the distance between the wing and strut is large. Near the wing-strut juncture location, a suction peak appears on the lower surface of the wing for the wing-strut configuration. The pressure difference between the wing-alone and wing-strut configurations decreases toward the outboard of the wing where the interference effects are diminished.

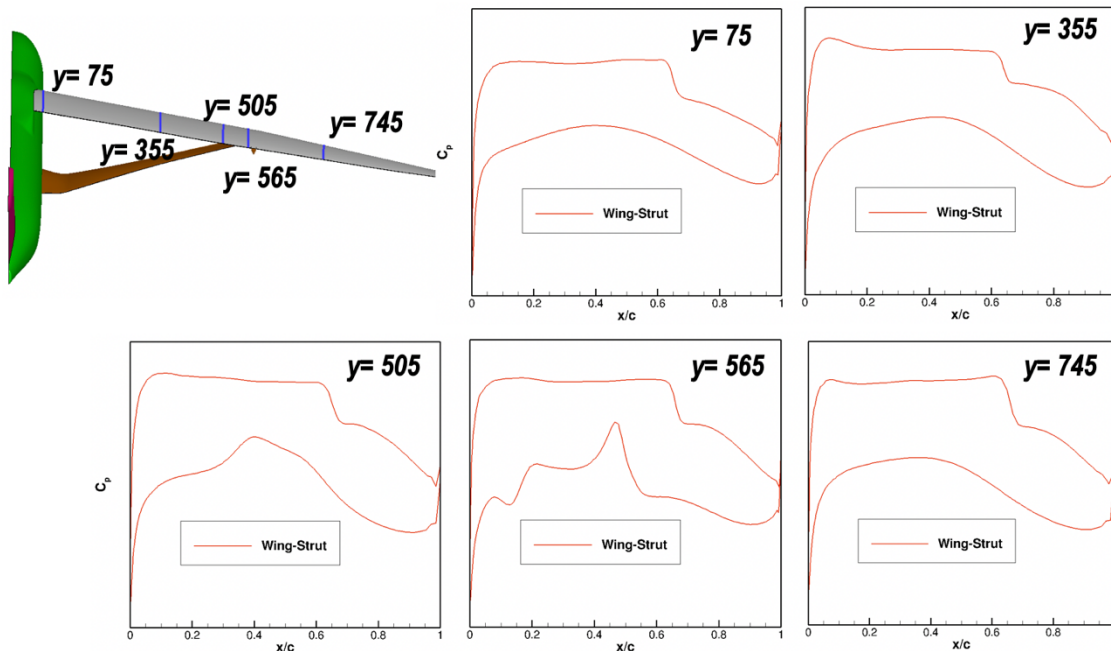


**Fig. 9 Comparison of Pressure Coefficient**  $(M_\infty = 0.8, \alpha = 1.533^\circ, Re = 14.0 \times 10^6)$

Figures 10 show the pressure coefficient distributions for the Mach 0.8 TTBW aircraft and Mach 0.745 TTBW aircraft at the design conditions. The Mach 0.745 was developed under a Phase III NRA contract funded by NASA AATT project. The presence of the strut underneath the wing induces a suction peak on the lower surface of the wing. The suction peak with steeper slope appears further back on the lower surface of the wing for the Mach 0.8 TTBW aircraft. The interference effects become more pronounced as the Mach number increases.

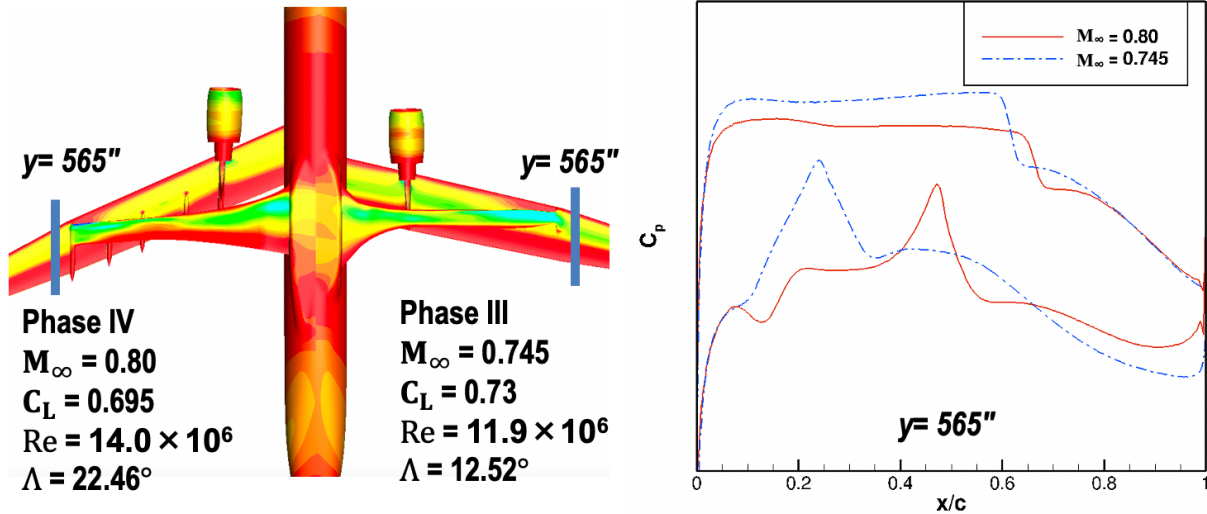


Fig. 10 Comparison of Pressure Coefficient for Mach 0.8 TTBW and Mach 0.745 TTBW aircraft

### C. Interference correction implementation

In this section a transonic wing-strut interference correction method is developed to correct the VSPAERO model coupled to the TSD/IBL method using the FUN3D simulation data. VSPAERO is a potential flow solver which has been implemented with a 2D transonic and viscous flow corrections via the TSD/IBL method. More details about VSPAERO coupled with the TSD/IBL method can be found in Ref. 3.

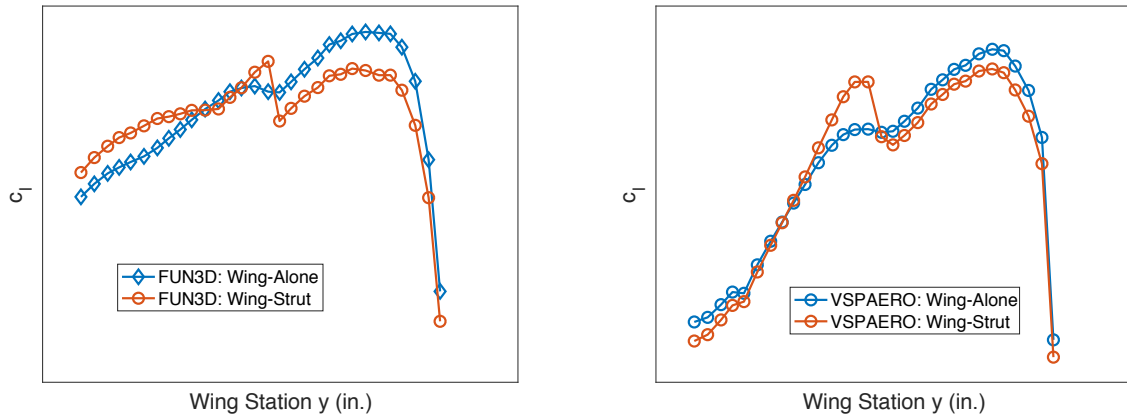
The wing-strut interference effects are calculated by determining the difference in the wing sectional aerodynamic coefficients between the wing-alone and the wing-strut configurations as shown in Fig. 4. The correction terms are calculated by using the following equation,

$$\Delta C_{IC} = \Delta C_{FUN3D} - \Delta C_{VSPAERO+TSD/IBL} \quad (1)$$

where  $\Delta C_{FUN3D}$  represents the change in the aerodynamic coefficient  $c$  which could be  $c_l$ ,  $c_d$ , and  $c_m$  between the wing-strut and the wing-alone configurations computed by FUN3D and  $\Delta C_{VSPAERO+TSD/IBL}$  represents the change in the aerodynamic coefficient  $c$  computed by VSPAERO+TSD/IBL.

Figure 11 shows the sectional lift coefficient distribution along the wingspan for Mach number 0.8, lift coefficient of 0.65, and Reynolds number of 14.0 million. The presence of the strut enhances the shock wave at the upper surface of the wing at inboard wing stations which increases the lift coefficient. There is an abrupt change in the lift coefficient near the wing-strut juncture location which is caused by the suction peak on the lower surface of the wing. The lift coefficient difference decreases toward the outboard of the wing where the interference effects are diminished. Figure 12 shows the sectional lift coefficient correction along the wingspan for the Mach 0.8 TTBW aircraft and the Mach 0.745 TTBW aircraft. The sectional lift

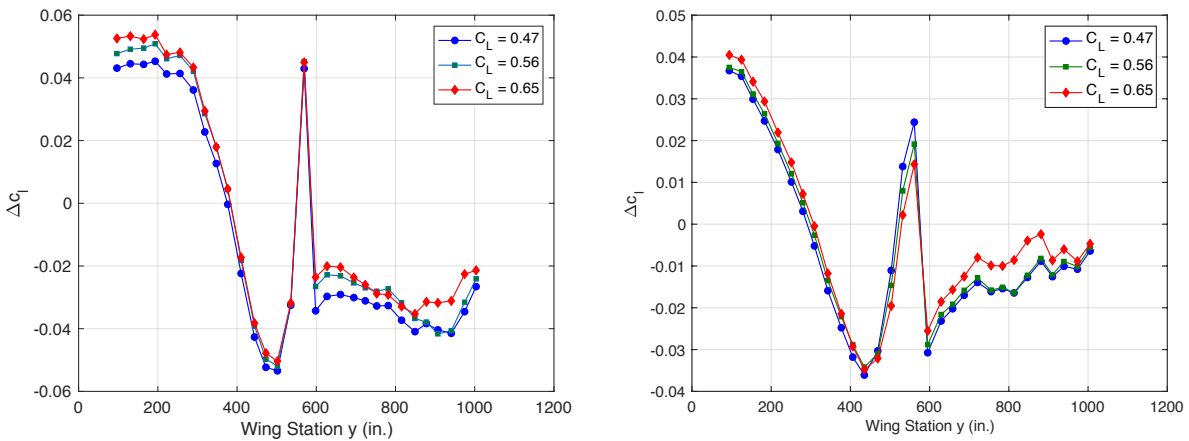
coefficient corrections are larger for the Mach 0.8 TTBW aircraft because the interference effects become more pronounced as the Mach number increases.



(a) Lift Coefficient Distribution - FUN3D

(b) Lift Coefficient Distribution - VSPAERO

**Fig. 11 Lift Coefficient Distribution ( $M_\infty = 0.8$ ,  $C_L=0.65$ ,  $Re = 14.0 \times 10^6$ )**

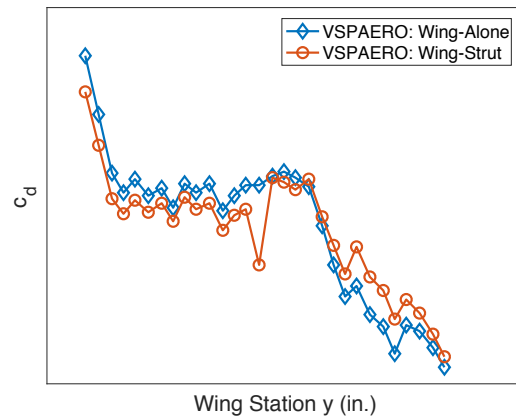
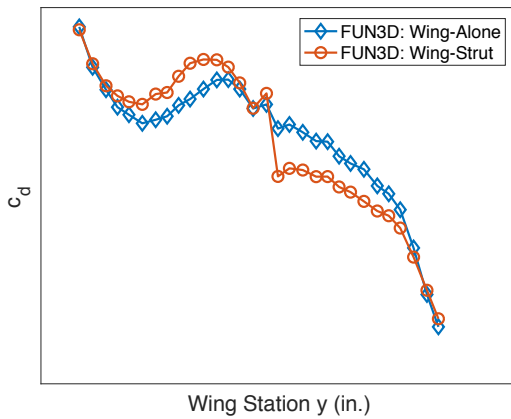


(a) Mach 0.8 TTBW

(b) Mach 0.745 TTBW

**Fig. 12 Lift Coefficient Correction Distribution between FUN3D and VSPAERO**

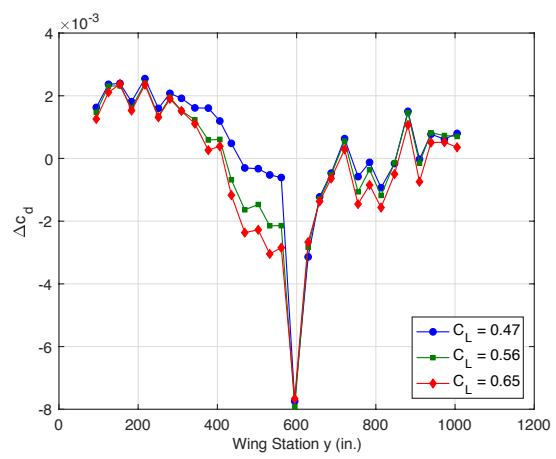
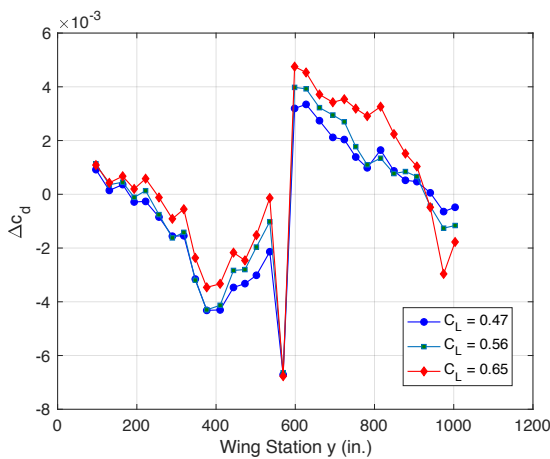
Figure 13 shows the sectional drag coefficient distribution along the wingspan for Mach number 0.8, lift coefficient of 0.65, and Reynolds number of 14.0 million. There is an abrupt change in the drag coefficient near the wing-strut juncture location which is caused by the suction peak on the lower surface of the wing. Figure 14 shows the sectional drag coefficient correction along the wingspan for the Mach 0.8 TTBW aircraft and the Mach 0.745 TTBW aircraft. The sectional drag coefficient corrections are larger at the outboard of the wing-strut juncture location for the Mach 0.8 TTBW aircraft.



(a) Drag Coefficient Distribution - FUN3D

(b) Drag Coefficient Distribution - VSPAERO

**Fig. 13 Drag Coefficient Distribution ( $M_\infty = 0.8$ ,  $C_L = 0.65$ ,  $Re = 14.0 \times 10^6$ )**

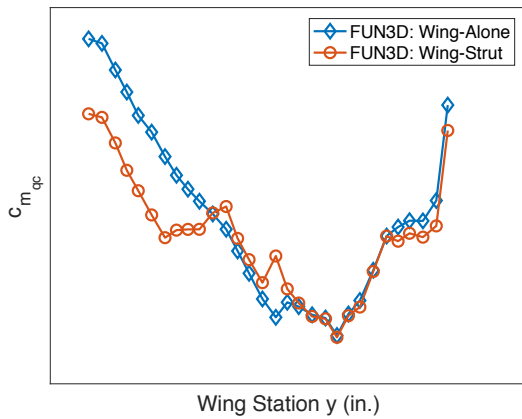


(a) Mach 0.8 TTBW

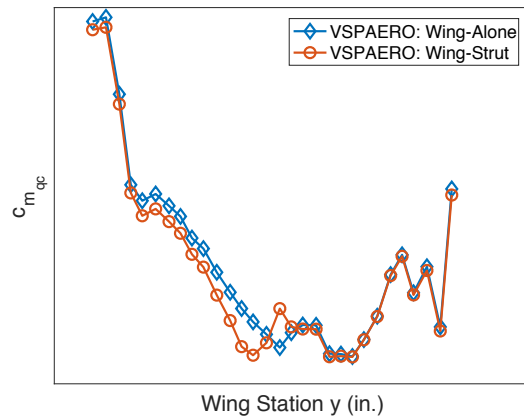
(b) Mach 0.745 TTBW

**Fig. 14 Drag Coefficient Correction Distribution between FUN3D and VSPAERO**

Figure 15 shows the sectional pitching moment coefficient distribution along the wingspan for Mach number 0.8, lift coefficient of 0.65, and Reynolds number of 14.0 million. The pitching moment coefficient is calculated about the quarter chord location. The presence of the wing-strut juncture changes the pitching moment coefficient at the inboard wing stations and near the wing-strut juncture location for the Mach 0.8 TTBW aircraft. Figure 16 shows the sectional pitching moment coefficient correction along the wingspan for the Mach 0.8 TTBW aircraft and the Mach 0.745 TTBW aircraft. The presence of the wing-strut juncture changes the pitching moment coefficient near the wing-strut juncture location for both the Mach 0.8 TTBW aircraft and Mach 0.745 TTW aircraft. However, the presence of the strut also changes the pitching moment coefficient at inboard wing stations for the Mach 0.8 TTBW aircraft.

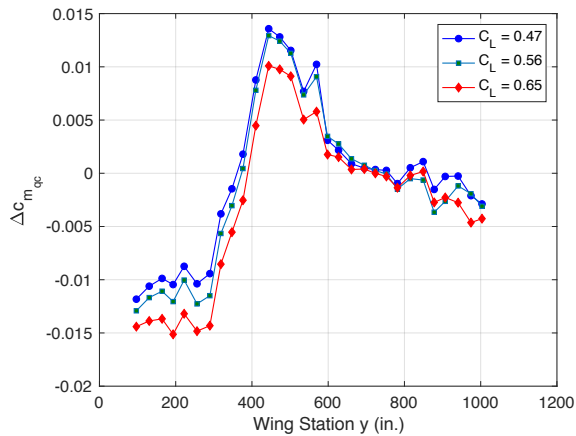


(a) Moment Coefficient Distribution – FUN3D

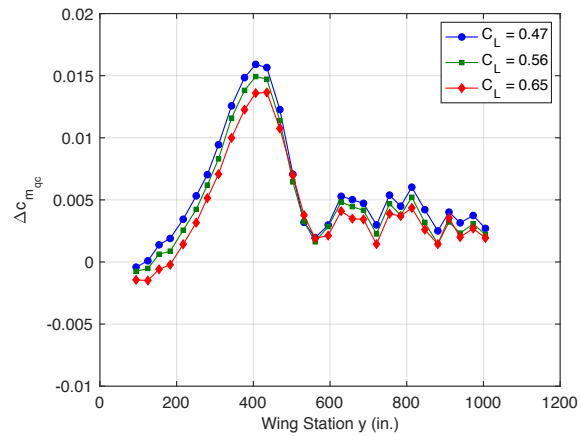


(b) Moment Coefficient Distribution – VSPAERO

**Fig. 15 Pitch Moment Coefficient ( $M_\infty = 0.8$ ,  $C_L=0.65$ ,  $Re = 14.0 \times 10^6$ )**



(a) Mach 0.8 TTBW



(b) Mach 0.745 TTBW

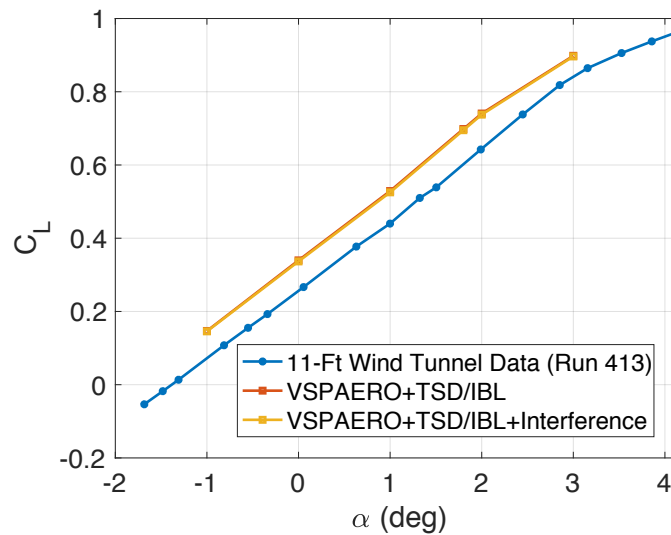
**Fig. 16 Pitch Moment Coefficient Correction Distribution between FUN3D and VSPAERO**

The correction method is applied to the VSPAERO+TSD/IBL model to update the sectional lift, drag, and pitching moment coefficients of each wing section. As can be seen, near the strut juncture region, there is a significant change in aerodynamic performance. The wing-strut interference correction is generally larger for the Mach 0.8 TTBW aircraft compared with the Mach 0.745 TTBW aircraft. The previous study<sup>5</sup> shows there is less impact of the Reynolds number effect on the interference. The developed correction model can be applied for different Reynolds number flow conditions. With the interference correction terms applied, the VSPAERO+TSD/IBL model is used for the aerodynamic analysis of the cruise 1g shape Mach 0.8 TTBW aircraft. Figure 17 shows the lift and drag coefficients computed by VSPAERO for the Mach 0.8 and a Reynolds number of 2.17 million. The differences between the simulation results of VSPAERO+TSD/IBL model with and without interference corrections are small. The computed results are compared to Run 378 wind tunnel data. While the lift coefficient is somewhat overpredicted, with the corrections applied to the VSPAERO model for transonic viscous flow and wing-strut interference aerodynamics, the lift and drag coefficients match well with the wind tunnel data, although there is a small discrepancy in the drag polar at lower lift coefficients, which is also seen with FUN3D model. Figure 18 shows the lift and drag coefficients computed by VSPAERO for the Mach 0.8 and a Reynolds number of 3.3 million and Run 413 wind tunnel data. The lift coefficient is also overpredicted. Overall, the lift and

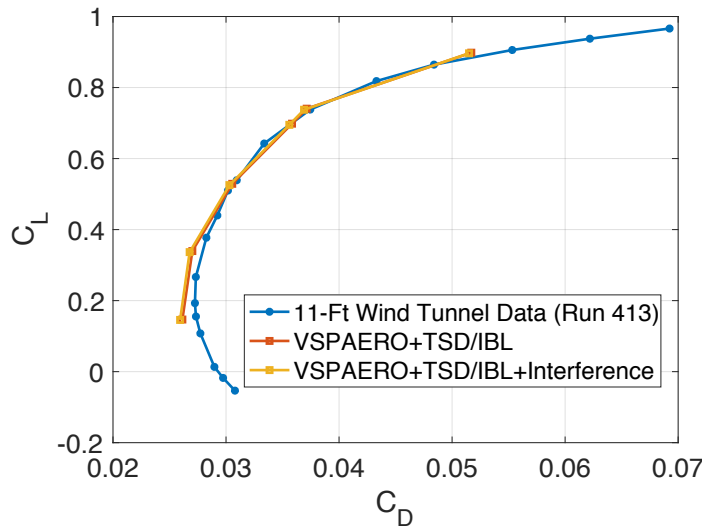
drag coefficients match well with the wind tunnel data. The good agreement between the VSPAERO model with corrections and the Run 378 and Run 413 wind tunnel data thus validates the aerodynamic modeling approach. Table 1 shows the interference corrections for the lift and drag coefficients at design lift coefficient of 0.695 and Reynolds number of 2.17 million. The interference corrections for the lift and drag coefficients are -0.0033 and -0.00024, respectively. The interference corrections are relatively small. The VSPAERO+TSD/IBL with the wing-strut interference correction model can be used as a rapid and reliable tool for the TTBW aircraft conceptual analysis and design.

**Table 1 Interference Corrections for  $C_L = 0.695$  and  $Re = 2.17 \times 10^6$**

	VSPAERO + TSD/IBL	+ Interference	Total
$C_L$	0.6983	-0.0033	0.695
$C_D$	0.0378	-0.00024	0.0376

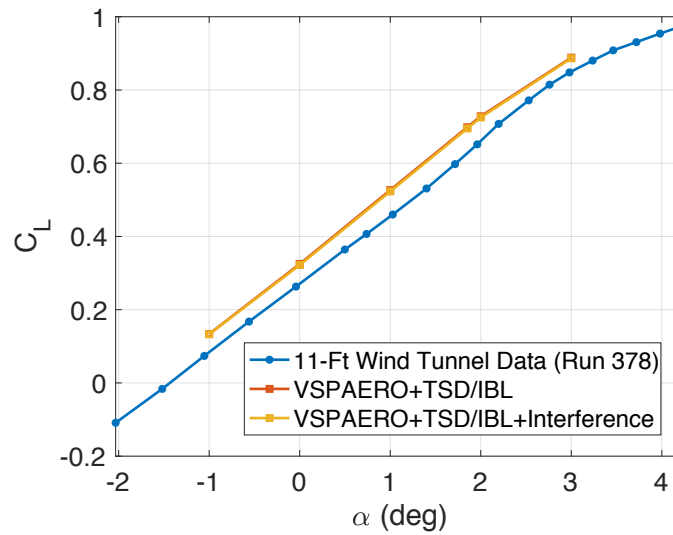


**(a) Lift curve**

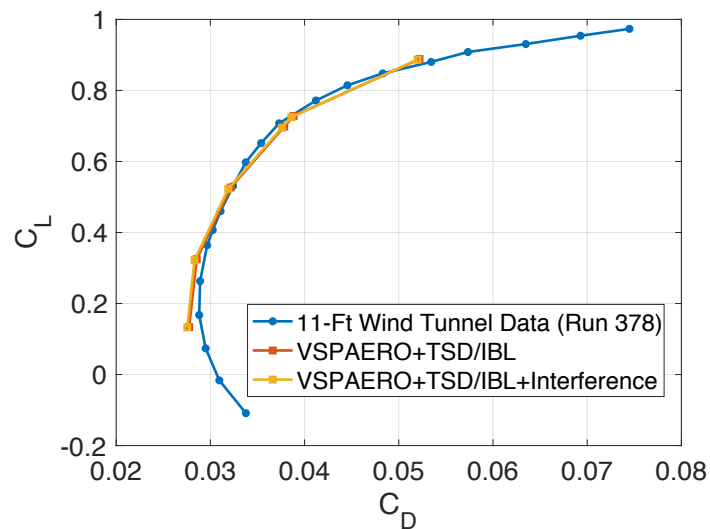


**(b) Drag Polar**

**Fig. 17 Lift Curve and Drag Polar ( $M_\infty = 0.8$ ,  $Re = 2.17 \times 10^6$ )**



(a) Lift Curve



(b) Drag Polar

Fig. 18 Lift Curve and Drag Polar ( $M_\infty = 0.8$ ,  $Re = 3.3 \times 10^6$ )

#### IV. Conclusions

A computational investigation of the wing-strut interference effect for the Mach 0.8 TTBW aircraft is presented. The presence of the strut underneath the wing induces a suction peak on the lower surface of the wing, which causes an abrupt change in aerodynamic forces and moments. The interference corrections for the Mach 0.8 TTBW aircraft are stronger than found for the Mach 0.745 TTBW aircraft. With the developed interference correction method in conjunction with the transonic viscous flow corrections via the TSD/IBL method, the VSPAERO model can be used as a reliable tool for the TTBW aircraft analysis and design.

## Acknowledgment

The authors wish to acknowledge NASA Advanced Air Transport Technology project for the funding support of this work. The authors also acknowledge Boeing Research and Technology and in particular Christopher Droney, Neal Harrison, Michael Beyar, Eric Dickey, and Anthony Sclafani, along with the NASA technical POC, Gregory Gatlin, for their research conducted under the NASA BAART contracts NNL10AA05B and NNL16AA04B. The research published in this paper is made possible by the technical data and wind tunnel test data furnished under these BAART contracts.

## References

1. Bradley, M. K. and Droney, C. K., "Subsonic Ultra Green Aircraft Research: Phase I Final Report," NASA Contractor Report NASA/CR-2011-216847, Boeing Research and Technology, April 2011
2. Bradley, M. K., Droney, C. K., and Allen, T. J., "Subsonic Ultra Green Aircraft Research Phase II: N+4 Advanced Concept Development," NASA Contractor Report NASA/CR-2012-217556, Boeing Research and Technology, May 2012
3. Nguyen, N., Fugate, J., Xiong, J. and Kaul, U., "Flutter Analysis of the Transonic Truss-Braced Wing Aircraft Using Transonic Correction", AIAA SciTech conference, AIAA-2019-0217, San Diego, CA, Jan. 2019
4. Fugate, J., Nguyen, N. and Xiong, J. "Aero-Structural Modeling of the Truss-Braced Wing Aircraft Using Potential Method with Correction Methods for Transonic Viscous Flow and Wing-Strut Interference Aerodynamics", AIAA Aviation conference, Dallas, TX, June. 2019
5. Xiong, J., Nguyen, N., and Fugate, J., "Investigation of Truss-Braced Wing Aircraft Transonic Wing-Strut Interference Effects Using FUN3D," AIAA Aviation Conference, AIAA-2019-3026, June 2019.
6. Biedron, R. T., et al. "FUN3D Manual 13.2", NASA TM-2017-219661, Aug. 2017
7. Lee-Rausch, E. M., Hammond, D. P., Nielsen, E. J., Pirzadeh, S. Z., and Rumsey, C. L., "Application of the FUN3D Unstructured-Grid Navier-Stokes Solver to the 4<sup>th</sup> AIAA Drag Prediction Workshop cases," AIAA Paper 2010-4511, June. 2010.
8. Roe, P. L., "Approximate Riemann Solvers, Parameter Vectors and Difference Schemes," *Journal of Computational Physics*, Vol. 46, No. 2, 1980, pp. 357–378
9. Venkatakrishnan, V., "Convergence to Steady State Solutions of the Euler Equations on Unstructured Grids with Limiters," *Journal of Computational Physics*, Vol. 118, No. 1, 1995, pp. 120–130
10. Spalart, P. R. and Allmaras, S. R., "A One-Equation Turbulence Model for Aerodynamic Flows," AIAA 1992-0439, Jan. 1992.